Investigation of atmospheric clouds and boundary layer dynamics during a dust storm in the Western-Indian region

Dharmendra Kumar Kamat, Som Kumar Sharma, Prashant Kumar, Kondapalli Niranjan Kumar, Sourita Saha, Hassan Bencherif

Investigation of atmospheric clouds and boundary layer dynamics during a dust storm in the Western-Indian region

Dharmendra Kumar Kamat [a,b], Som Kumar Sharma [a,*,1], Prashant Kumar [c], Kondapalli Niranjan Kumar [d], Aniket [a], Sourita Saha [e], Hassan Bencherif [f]

[a] *Physical Research Laboratory, Ahmedabad, India*
[b] *Indian Institute of Technology Gandhinagar, Gandhinagar, India*
[c] *Space Applications Centre, Ahmedabad, India*
[d] *NCMRWF, Noida, India*
[e] *Scripps Institution of Oceanography, University of California, San Diego, CA, USA*
[f] *University De la Reunion, Reunion Island, France*

A B S T R A C T

This study investigates the dynamics of atmospheric clouds and boundary layer due to a sudden dust storm over Ahmedabad (23.02° N, 72.57° E), a Western-Indian region, during the pre- monsoon season on May 13, 2024. The storm was triggered by the outflow from convective systems originating in southwest Gujarat and southeast Rajasthan, combined with the significant deepening of the thermal low core over Ahmedabad, which generated strong near-surface winds and initiated the dust storm. These systems and the dust storm were captured by the INSAT-3D satellite and MODIS instrument on NASA's Aqua and Terra satellites. The ground-based Ceil-ometer Lidar backscatter profile showed an abrupt change in the mixed layer height (MLH) from ~2.5 km to about 250 m during the storm due to attenuation of the signal by heavy dust load. The MLH, ~2 km on 12 May (previous day), shallowed to ~800 m on 14 May (post dust storm day), with increased backscatter indicating high dust concentration. Vertical visibility dropped to 340–660 m during the dust storm. During the storm, relative humidity near the surface increased from 29% to 48% due to moisture transport by frontal system along the density current pathway, while near-surface wind speeds peaked at around 6–10 m/s. After the storm, deep convective clouds formed with a vertical extent of ~11 km, resulting in approximately 19 mm of rainfall with nearly 15 mm falling within just 1 h indicating the dust-cloud interaction. This study highlights the impact of moist convection and subsequent dust storm on clouds and boundary layer dy-namics, emphasizing the importance of ground-based instruments, satellites, and reanalysis datasets in atmospheric monitoring. Understanding the causes, mechanisms, and consequences of dust storms is critical for mitigating their effects and adapting to the changing climate patterns that may influence their frequency and intensity.

A R T I C L E I N F O

Keywords: Dust storm Boundary layer Mixed layer Clouds Lidar MODIS VIIRS

* Corresponding author. Space and Atmospheric Sciences Division, Physical Research Laboratory (PRL), Navrangpura, Ahmedabad, 380009, India.
E-mail addresses: somkumar@prl.res.in, sharmasomkumar@gmail.com (S.K. Sharma).
[1] URL: http://www.prl.res.in/~somkumar.

https://doi.org/10.1016/j.rsase.2024.101442

1. Introduction

Dust storms are meteorological phenomena characterized by strong winds that lift and transport loose sand and dust particles from the ground into the atmosphere over vast distances (Goudie, 2009). These events are predominantly observed in arid and semi-arid regions where sparse vegetation and low moisture levels facilitate easy wind transport of surface materials (Shao and Dong, 2006). The repercussions of dust storms extend well beyond their origin, impacting atmospheric conditions, human health, and ecological systems globally. Mineral dust aerosols play a crucial role in Earth's radiation budget by interacting with incoming solar radiation (Slingo et al., 2006; Kedia et al., 2018; Fountoukis et al., 2020), thereby influencing weather patterns and climate dynamics. Moreover, dust particles serve as nuclei for cloud condensation and ice formation, influencing cloud properties and precipitation patterns (Möhler et al., 2006; Kumar et al., 2009; Karydis et al., 2011). The implications for human health are also profound, as dust storms degrade air quality and can transport pathogenic microorganisms, leading to respiratory and cardiovascular diseases (Zhang et al., 2016; Khaniabadi et al., 2017; Goudie, 2020; Aghababaeian et al., 2021; Jasim et al., 2022).

Dust storms have been investigated over the several parts of India including the Northern India Indo-Gangetic plains, and Western Ghats (Kumar et al., 2015; Dumka et al., 2019; Banerjee et al., 2021; Chakravarty et al., 2021; Singh et al., 2022; Shukla et al., 2022; Parambil et al., 2023). The interaction of mineral dust with clouds and precipitation have great impact on the climate of arid and semi-arid regions (Huang et al., 2014). This study investigates the characteristics of a sudden dust storm and its effect on the atmospheric clouds and boundary layer over a semi-arid Western-Indian region Ahmedabad. The semi-arid regions of Western India, including Ahmedabad, frequently experience dust storms during the post-monsoon season, originating from the Thar desert in Rajasthan (Santra et al., 2018).

Several studies in past have investigated these dust storms over the western-Indian region (Prakash et al., 2013; Chhabra et al., 2021; Saha et al., 2022; Shukla et al., 2023; Chhabra et al., 2021) investigated the impact of dust storm on the aerosols optical and radiative properties and found a reduction in total downward surface flux leading to cooling effect. Saha et al. (2022) studied the impact of dust storm on atmospheric boundary layer. The study found a spike of 118.5% and 44.5% in PM_{10} and $PM_{2.5}$ concentrations during the dust storm compared to previous day. Another study by Shukla et al. (2023) reported twice increase in the ultraviolet aerosol index during a dust storm over the Western-Indian region compared to previous dust free day.

This study focuses on understanding the characteristics and impacts of a sudden dust storm over Ahmedabad, a semi-arid region in Western India (Fig. 1). Utilizing ground-based Lidar, satellite observations, weather sensors, radiosonde data, and reanalysis datasets, the study examines how dust storms affect boundary layer dynamics and cloud formation. Specifically, the study utilizes the backscatter signals from a ground-based Ceilometer Lidar at the Physical Research Laboratory, Ahmedabad, to analyze boundary layer and cloud characteristics during the dust storm. The collocated weather sensor is used to study the surface meteorological conditions during the dust storm. Satellite observation provide large scale dynamics of dust and clouds, and also the microphysical properties of clouds. Combining, these datasets we have comprehensively studied a pre-monsoon dust storm over the Ahmedabad region. The rest of the paper is structured as follows. Section 2 describes the datasets used in the study. Results are discussed in Section 3. Summary and conclusions are presented in Section 4.

2. Datasets

2.1. Ceilometer Lidar

The Ceilometer (Vaisala CL31) is low power eye-safe Lidar that uses Indium Gallium Arsenide (InGaAs) laser to transmit an infrared signal at 910 nm vertically up in the atmosphere. The backscattered signal after reflection from the haze, fog, mist, virga, precipitation, aerosols, and clouds is used to calculate the boundary layer structure and cloud bases (Münkel et al., 2007). The vertical and temporal resolution of the Ceilometer Lidar used in this study is 10 m and 16 s, respectively. This Lidar can probe the atmosphere to detect the cloud base height up to about 7.6 km. In this study, we have used the Lidar backscatter signal to investigate the dynamics of boundary layer during the dust storm. The gradient of backscatter between the boundary layer and free troposphere is used to calculate the boundary layer or mixing layer height. The boundary layer height is derived using the gradient method (Münkel et al., 2007; Lo Feudo et al., 2020). In this method, the gradient of the backscatter signal is calculated for each vertical level and the height corresponding to the minimum gradient is assigned as the boundary layer height. The gradient of backscatter is calculated using equation (1).

$$\frac{\partial \beta}{\partial h}(h_i) = \frac{\beta(h_i + \Delta h) - \beta(h_i - \Delta h)}{2\Delta h} \tag{1}$$

where, β is the backscattered signal ($m^{-1}sr^{-1}$), h_i is the height above the Ceilometer, and Δh is the vertical resolution (10 m).

2.2. Weather transmitter

The WXT536 weather transmitter is a weather sensor capable of measuring atmospheric pressure, temperature, humidity, rain, and wind. It basically consists of a PTU (Pressure Temperature Humidity) module, a rain sensor, and a wind sensor. The PTU module consists of a capacitive silicon sensor for pressure measurement, resistive thin film sensor for temperature measurement, and capacitive thin film polymer sensor for humidity measurement. The rain is measured using the piezoelectric effect and wind is measured using 3 equally spaced ultrasonic transducers. This weather sensor is collocated with the Ceilometer Lidar and measures the

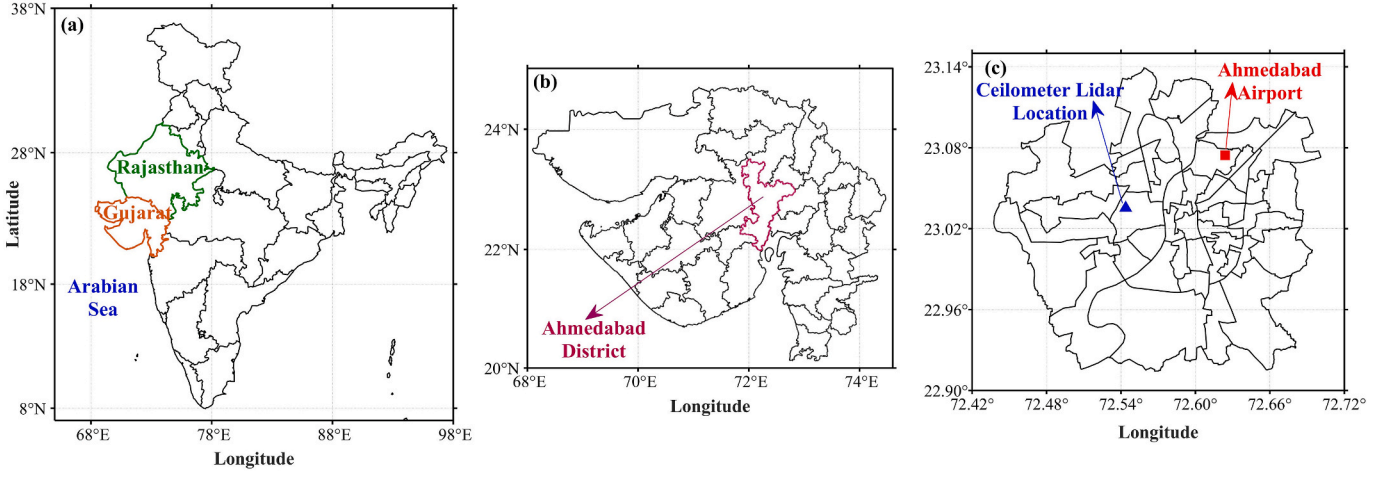

Fig. 1. (a) Map of India highlighting the western states of Gujarat and Rajasthan. (b) Gujarat with Ahmedabad district highlighted. (c) A close-up view of Ahmedabad city, marking the Ceilometer Lidar operational site (blue triangle) and Ahmedabad airport, the location for radiosonde launches (red square).

pressure, temperature, relative humidity, rain, and wind every minute.

2.3. INSAT-3D

INSAT-3D is a geostationary satellite launched by Indian Space Research Organization (ISRO) in 2013 for meteorological observations. It has a 6-channel (visible, near-infrared, midwave infrared, water vapor, and two split-window infrared channels) multispectral imager and 19 channel sounder (Kumar and Shukla, 2019). INSAT-3D is positioned at 82 °E over the Indian ocean. In this study, we have used INSAT-3D imager brightness temperature data over the Western-Indian region. These datasets are available at 30-min resolution.

2.4. MODIS

The Moderate Resolution Imaging Spectroradiometer (MODIS) is one of the instruments onboard National Aeronautics and Space Administration (NASA) satellites Terra and Aqua launched in 1999 and 2002, respectively. The MODIS instrument captures the entire Earth in every 1–2 days in 36 spectral bands ranging from 0.4 μm to 14.4 μm. In this study, we have used the MODIS surface reflectance (Liang et al., 2002) and cloud properties (Platnick et al., 2003) datasets over the western-Indian region.

2.5. VIIRS

The Visible Infrared Imaging Radiometer Suite (VIIRS) is onboard two satellites: NASA Suomi-national polar-orbiting partnership (SNPP) satellite and National Oceanic and Atmospheric Administration - 20 (NOAA-20) satellite. SNPP satellite was launched in 2011 and NOAA-20) satellite was launched in 2017, and both these satellites circles the Earth in same orbit but is separated in space and time by 50 min (Cao et al., 2018). VIIRS is a visible and infrared radiometer with 22 spectral bands ranging between 0.41 and 12.5 μm, which are separated into 16 moderate and 5 imaging resolution bands (Chen et al., 2021). The spatial resolution of VIIRS is 375 m and 750 m for imaging and radiometric bands, respectively. We have used the cloud properties derived from the VIIRS on board SNPP and NOOA-20 satellites to study the cloud characteristics during the dust storm.

2.6. ERA5 reanalysis

European Centre for Medium-Range Weather Forecasting (ECMWF) Reanalysis v5 or ERA5 is the 5th generation of reanalysis products providing land, atmosphere, and ocean datasets. It provides hourly estimate of several atmospheric datasets from 1940 onwards on a regular grid of $0.25^\circ \times 0.25^\circ$ (Hersbach et al., 2020). This study uses the ERA5 wind products on different pressure levels. These products are available at the climate data store of ECMWF.

3. Results and discussions

3.1. Satellite-based observation of dust storm and clouds

The brightness temperature imagery obtained from the INSAT-3D satellite on May 13, 2024, spanning from 0630 to 2300 UTC, is depicted in Fig. 2. Clouds observed using satellite imagery are identifiable by their higher reflectance and lower brightness temperature compared to the underlying surface (Frey et al., 2008). It can be clearly seen that around the observational site i.e., Ahmedabad (marked by a circle), two convections start forming, one toward the south-west and other in the north-east direction at 7:00 UTC. The clouds formed due to this convection started growing and covered the Ahmedabad region at 1100 UTC. The clouds persisted till next day morning. These clouds covered a large part of Rajasthan and Gujarat as inferred from the low brightness temperature of clouds. The India Meteorological Department (IMD) had issued a forecast predicting isolated to scattered, light to moderate rainfall accompanied by thunderstorms, lightning, and gusty winds (30–40 kmph) over the Gujarat region on 13 and May 14, 2024. Ahmedabad experienced a significant dust storm starting around 1140 UTC on May 13, 2024, subsiding by 1210 UTC, followed promptly by rainfall in the region. Such dust storms, driven by the outflow from moist convection, are typical during the pre-monsoon season (Knippertz, 2014). This study highlights a similar dust storm event triggered by moist convection over the Western Indian region on May 13, 2024. The INSAT-3D imagery effectively captured the evolution of convective systems leading to cloud formation and subsequent weather phenomena, underscoring the utility of satellite observations in understanding and predicting regional weather patterns.

Fig. 3 depicts the reflectance data retrieved from MODIS covering the Western-Indian region from 12 to May 14, 2024. Two passes of MODIS were obtained over Ahmedabad on each day. Clearly, low reflectance is seen over the Ahmedabad region on May 12, 2024 at 0430 and 0850 UTC. However, on May 13, 2024 at 0930 UTC, significant dust and cloud cover is evident near the Ahmedabad (marked by circle) region. Large patches of clouds and dust, several kilometers in size, were seen to the southwest and northeast, as shown by the high reflectance. On May 14, 2024, traces of high dust concentration were found over the Ahmedabad region.

This underscores the capability of both INSAT-3D and MODIS to capture atmospheric phenomena such as dust and cloud formations in this region. However, INSAT-3D holds a distinct advantage over MODIS due to its geostationary orbit, allowing for continuous monitoring and fewer gaps in observation, particularly beneficial for tracking the dynamic behavior of clouds and dust storms over time. This capability enhances the utility of INSAT-3D in providing detailed insights into meteorological and environmental conditions over the Western-Indian region.

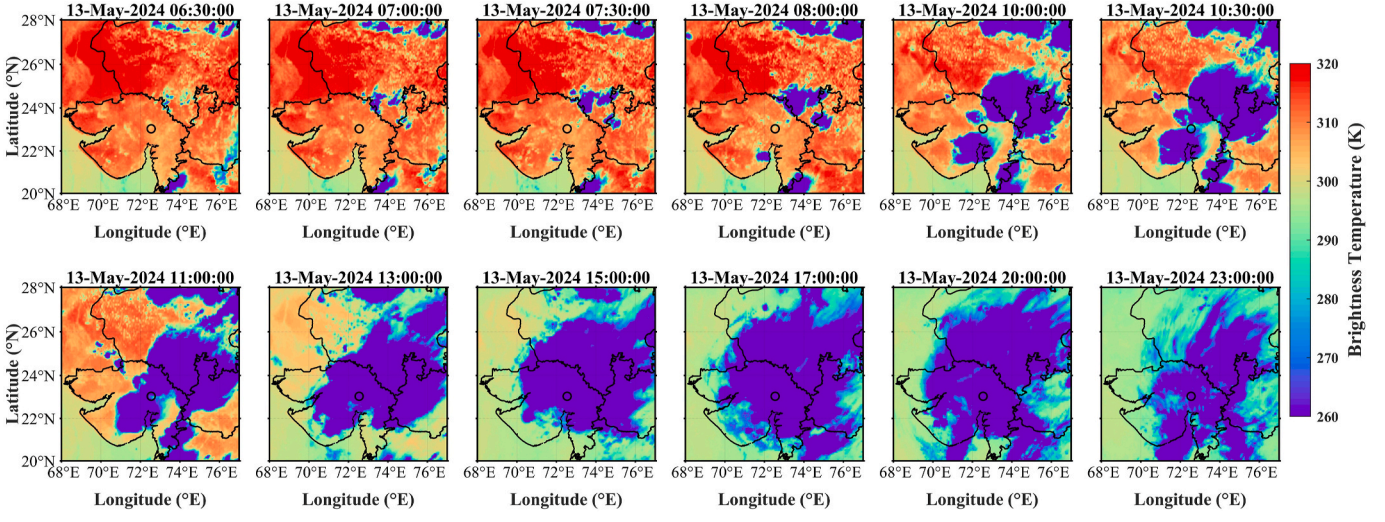

Fig. 2. Brightness temperature showing the occurrence of dust and clouds over the western-Indian region obtained from the INSAT-3D satellite on May 13, 2024.

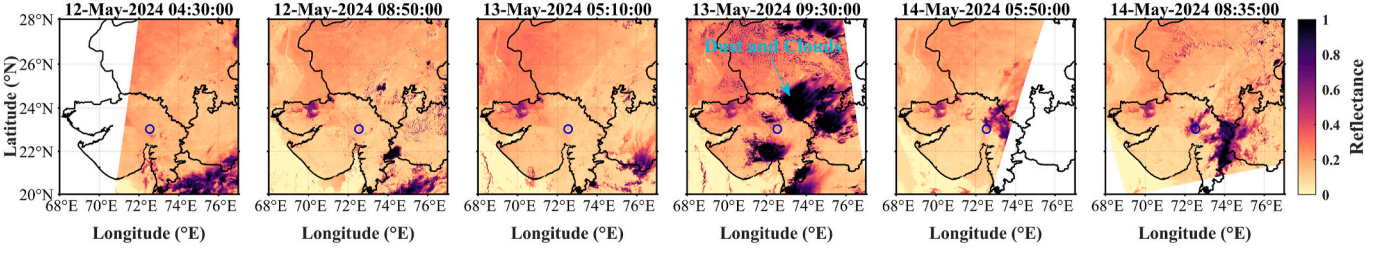

Fig. 3. Reflectance over the Western-Indian region obtained from MODIS during 12–14 May 2024. The high reflectance on May 13, 2024 at 0930 UTC indicates the presence of dust and clouds.

Satellite remote sensing techniques for monitoring dust storms have advanced significantly due to rapid improvements in satellite technology (Evan et al., 2006; Di et al., 2016; Sun et al., 2019). These methods primarily rely on detecting the reflectance differences between dust particles and the underlying surface or clouds in the visible and near-infrared bands, as well as the brightness temperature in thermal infrared bands (Sun et al., 2019). The reflectance of dust generally increases with wavelength between 0.4 and 2.5 μm, reaching a minimum in MODIS band 3 (0.469 μm) and a maximum in MODIS band 7 (2.13 μm). This spectral characteristic of sand facilitates distinguishing sand and dust storms from clouds, as clouds have their highest reflectance in MODIS band 3 (Qu et al., 2006). However, in case such as this study, when the dust storm is covered by thick clouds, it is difficult to completely monitor the dust information. To address these limitations, ground-based instruments offer a complementary approach to monitor dust storm characteristics more comprehensively. In this study, ground-based Ceilometer Lidar is employed to investigate cloud and boundary layer dynamics over the study region during dust storm. Ceilometer Lidar provides detailed vertical profiles of aerosols and clouds, offering valuable insights into the atmospheric conditions that influence dust storm formation and behavior. This integration of ground-based Ceilometer Lidar with satellite remote sensing enhances our ability to capture a more complete picture of dust storm dynamics, especially in scenarios where satellite observations may be hindered by cloud cover. The following section will delve into the specific methodologies and findings from the ground-based observations, contributing to a deeper understanding of dust storm phenomena and their environmental impacts.

3.2. Clouds and boundary layer dynamics

This section investigates the influence of a dust storm on the atmospheric clouds and boundary layer (ABL) using backscatter received from Ceilometer Lidar over the Ahmedabad region from 12 to May 14, 2024 (Fig. 4a–c). The backscatter signal is normalized to distinguish the mixed layer from the free troposphere, prominently displays strong signals from the lower troposphere, indicative of the ABL. The boundary layer height (BLH) is delineated by a black line in Fig. 4a–c. To determine the BLH, we performed the gradient analysis, outlier removal, interpolation for missing values, and smoothing of raw backscatter signal. A well-defined boundary layer was evident on May 12, 2024, with the BLH peaking at approximately 2 km during daytime, followed by a stable nocturnal ABL. The following day saw rapid growth of the ABL, with the BLH reaching about 2.5 km by 1000 UTC, although it began collapsing around 1140 UTC due to the onset of a severe dust storm (Fig. 4b). The dust storm disrupted the ABL, followed by subsequent rainfall. Post-rain, a thick nocturnal boundary layer began forming around 0600 UTC. By May 14, 2024, the ABL started rebuilding, albeit with a shallower BLH peaking at only about 800 m. The nocturnal BLH was also reduced compared to previous days due to decreased temperatures.

The formation and behavior of the ABL are influenced by temperature and relative humidity, with surface temperature directly impacting BLH (Garratt, 1994). The rainfall following the dust storm on May 13, 2024 cooled temperatures over Ahmedabad, contributing to the lower BLH observed on May 14, 2024. Fig. 4d–f illustrate cloud base height (CBH) and vertical visibility over the study site during 12–14 May 2024. On May 12, 2024, sparse cloud occurrences were observed at various heights. However, after the dust storm on May 13, 2024, clouds covered the Ahmedabad region, accompanied by subsequent rainfall. Notably, clouds with a CBH of approximately 2.7 km formed at 1210 UTC and ascended to 7.6 km by 2300 UTC. During the dust storm, vertical visibility ranged from 340 m to 660 m. The sudden collapse of the boundary layer caused by a dust storm has been previously studied by (Saha et al., 2022).

Fig. 5 illustrates the impact of the dust storm and subsequent rain on the ABL. The dust storm event is demarcated between two white dashed lines. A notable, abrupt disruption in the ABL is evident at 1140 UTC coinciding with the onset of the dust storm. Prior to this event, the ABL had developed into a well-defined mixed layer with a Boundary Layer Height (BLH) of approximately 2.5 km. Up until 1140 UTC, strong backscatter indicative of the mixed layer extended from the surface up to about 2.5 km. With the commencement of the dust storm, the strong backscatter characteristic of the mixed layer was restricted to the lower atmosphere, specifically up to only 250 m above the ground. This attenuation of the lidar signal within the lower 250 m was primarily due to the heavy loading of dust particles in lowest ABL. The dust appeared concentrated near the ground, resembling a density current in the lowest troposphere, suggesting its local origin rather than long-distance transport. The arrival of cold front affects the ABL making it shallower due to the compression of the boundary layer by the intrusion of cold air (Choi et al., 2008). Following the dust storm, clouds formed around 1210 UTC with a Cloud Base Height (CBH) of approximately 2.7 km, persisting into the next morning. Rainfall began at 1218 UTC and continued until 1754 UTC. The rain dissipated the mixed layer and facilitated the settling of dust particles, resulting in a residual layer that was considerably weaker compared to the day before. In the next section, the genesis and cause of dust storm is discussed.

3.3. Synoptic meteorological conditions

The synoptic meteorological conditions during the dust storm were analyzed using mean sea level pressure (MSLP) and wind maps derived from the ERA5 reanalysis. Fig. 6 illustrates the variation in MSLP over the western Indian region on May 13, 2024, from 0900 UTC to 1300 UTC. A notable deepening of the thermal low (a low-pressure area formed due to intense surface heating) is observed around the Ahmedabad region between 1000 UTC and 1200 UTC, with dissipation occurring afterward. The significant deepening of the thermal low core over Ahmedabad was crucial in triggering strong near-surface winds, which initiated the dust storm in the study area. Several pre-monsoon dust storms have been associated with similar synoptic meteorological patterns, characterized by low-pressure systems centered over the Thar Desert and the western Indo-Gangetic Plain (Sharma et al., 2012; Kumar et al., 2014, 2015; Dumka et al., 2019). Dumka et al. (2019) previously reported a similar phenomenon that triggered a dust storm over northern

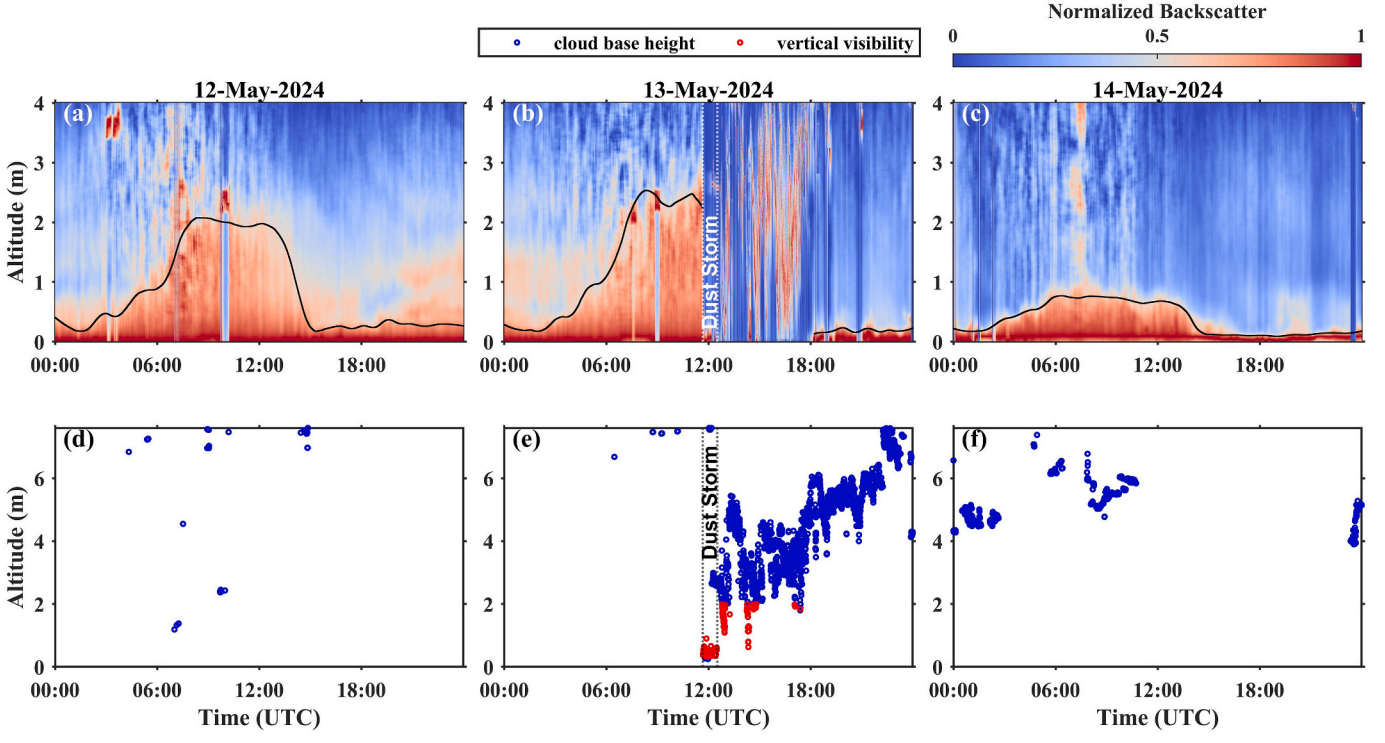

Fig. 4. (a–c) Boundary layer profile derived from the backscatter signal received from the Ceilometer Lidar at the Physical Research Laboratory, Ahmedabad during 12–14 May 2024. (d–f) shows the cloud base height (blue circle) and vertical visibility (red circle). The dust storm event is marked between the two white dotted line in (e) and (f).

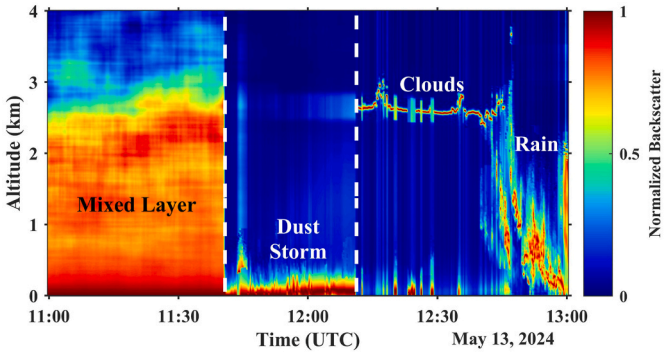

Fig. 5. Backscatter obtained from the Ceilometer Lidar over the Ahmedabad on May 13, 2024 from 1100 to 1300 UTC showing the mixed layer before the dust storm event and clouds and rain after the event.

India from 12 to 16 June 2018. Their study emphasized the presence of strong near-surface southwesterlies (~15–20 m/s), which were associated with the advancing monsoon flow in response to the thermal low deepening over the Thar Desert. Intense daytime heating over arid and semi-arid regions, like Ahmedabad, deepens the thermal low, fostering convective turbulence and mixing that re-distributes dust evenly within the boundary layer up to approximately 4 km (Kumar et al., 2014).

Additionally, ERA5 derived winds at 1000 hPa and 925 hPa on May 13, 2024, from 1000 UTC to 1200 UTC is shown in Fig. 7. The ERA5 derived winds shows westerlies with magnitude ~4–6 m/s over the Arabian Sea associated with the summer monsoon flow. The core of strong winds (>10 m/s) is seen to advance progressively inland towards the south-west Gujarat from the Arabian sea in response to the deepening of the heat low over the Ahmedabad region (Fig. 7a–c). These surface-level winds were instrumental in triggering the sudden onset of the dust storm. When strong near-surface winds in the monsoon flow move northward into semi-arid and arid regions (Gujarat and Rajasthan), they trigger dust emissions. This occurs as the monsoon flow behaves like a density current, driven by the density contrast between the cooler, moisture-laden monsoon air and the warm, dry air over these regions (Bou Karam et al., 2008). Fig. 7d–f shows the strong winds at 925 hPa near the south-east region in Rajasthan.

To identify the primary source of the dust storm, it is crucial to analyze wind pathways. The one-day back-trajectory of the air mass, computed using the HYSPLIT (Hybrid Single-Particle Lagrangian Integrated Trajectory) model (Stein et al., 2015), is illustrated in Fig. 8. This trajectory, ending at 500 m above the surface over Ahmedabad and initiated every 3 h, reveals an influx of air masses originating from the Arabian Sea. These air masses pass through Gujarat and Rajasthan, as observed on May 13, 2024, between 1000 UTC and 1200 UTC. Notably, the air masses enter Gujarat from the south and reach Ahmedabad at 1000 UTC and 1100 UTC, aligning well with the previously discussed wind patterns.

The meteorological conditions over the Ahmedabad region are also monitored using the weather station. Fig. 9a illustrates the surface temperature and pressure recorded from the local weather station between 12 and 14 May. On 12th May, the maximum surface temperature reached approximately 41 °C, followed by a slight increase to 42 °C on the 13 May. During the dust storm on the 13 May, the temperature sharply dropped from 41 °C to 33 °C, coinciding with a rise in atmospheric pressure from 998 hPa to 1001 hPa. This temperature decrease can be attributed to the reflective nature of dust particles, which attenuate incoming solar radiation (Choobari et al., 2014). Similar temperature drops following dust storms have been reported in several studies (Singh et al., 2022; Saha et al., 2022; Shukla et al., 2023). In this study, however, the dust storm was triggered by the arrival of a moist density current from the Arabian Sea. Consequently, the observed temperature decrease and pressure increase are primarily associated with cold air advection and the arrival of a frontal system along the density current pathway (Dumka et al., 2019; Wang et al., 2021). This finding is supported by wind patterns and air mass trajectories, which confirm the transport of moist air from the Arabian Sea, as discussed earlier. Subsequently, temperatures continued to decline through the following morning, with the peak temperature on the subsequent day decreasing by about 5 °C compared to the previous day. Fig. 9b depicts changes in relative humidity and rainfall over the observation period. Relative humidity surged from 29% to 48% during the dust storm, indicating the influx of moisture alongside airborne dust particles. Rainfall began immediately following the dust storm, accumulating around 19 mm from 1218 UTC to 1754 UTC, with nearly 15 mm falling within just 1 h between 1218 UTC and 1318 UTC (Fig. 9b). This intense rainfall resulted from deep convective cloud formation, as dust particles acted as cloud condensation nuclei (CCN), aiding water vapor condensation from the moist convection system that triggered the storm. Mineral dust can serve as effective CCN by facilitating water adsorption onto particle surfaces and can significantly increase precipitation (Yin et al., 2002; Karydis et al., 2011; Bangert et al., 2012; Huang et al., 2018). The interaction between dust and clouds, along with its impact on precipitation, is discussed in more detail in the next section. Fig. 9c presents a time series of surface wind speeds measured at Ahmedabad from 12 to May 14, 2024. The highest recorded surface wind speed using weather station during the dust storm peaked at 3.7 m/s (13.32 km/h). Comparatively, a previous study on a dust storm over Ahmedabad on April 27, 2021, reported a maximum wind speed of approximately 5 m/s (Saha et al., 2022). Similarly, another study by Shukla et al. (2023) reported a peak wind speed of 4 m/s during a dust storm on May 5, 2016. To further analyze the vertical profiles of temperature, pressure, relative humidity, and wind characteristics, we utilized radiosonde data.

The radiosonde launch site, located at Ahmedabad airport, is approximately 13 km from the Physical Research Laboratory, where the Ceilometer Lidar and weather stations are operational. Radiosondes are launched twice daily at 0000 UTC and 1200 UTC. Fig. 10

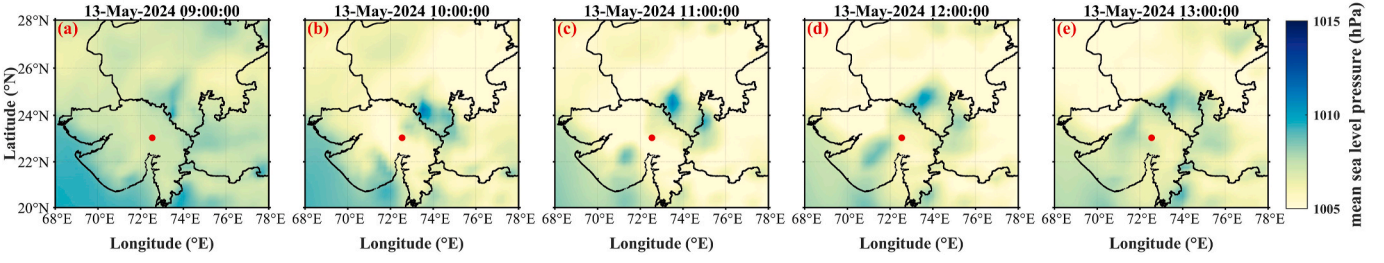

Fig. 6. Variation in mean sea level pressure (MSLP) over the western-Indian region during May 13, 2024, from 0900 UTC to 1300 UTC.

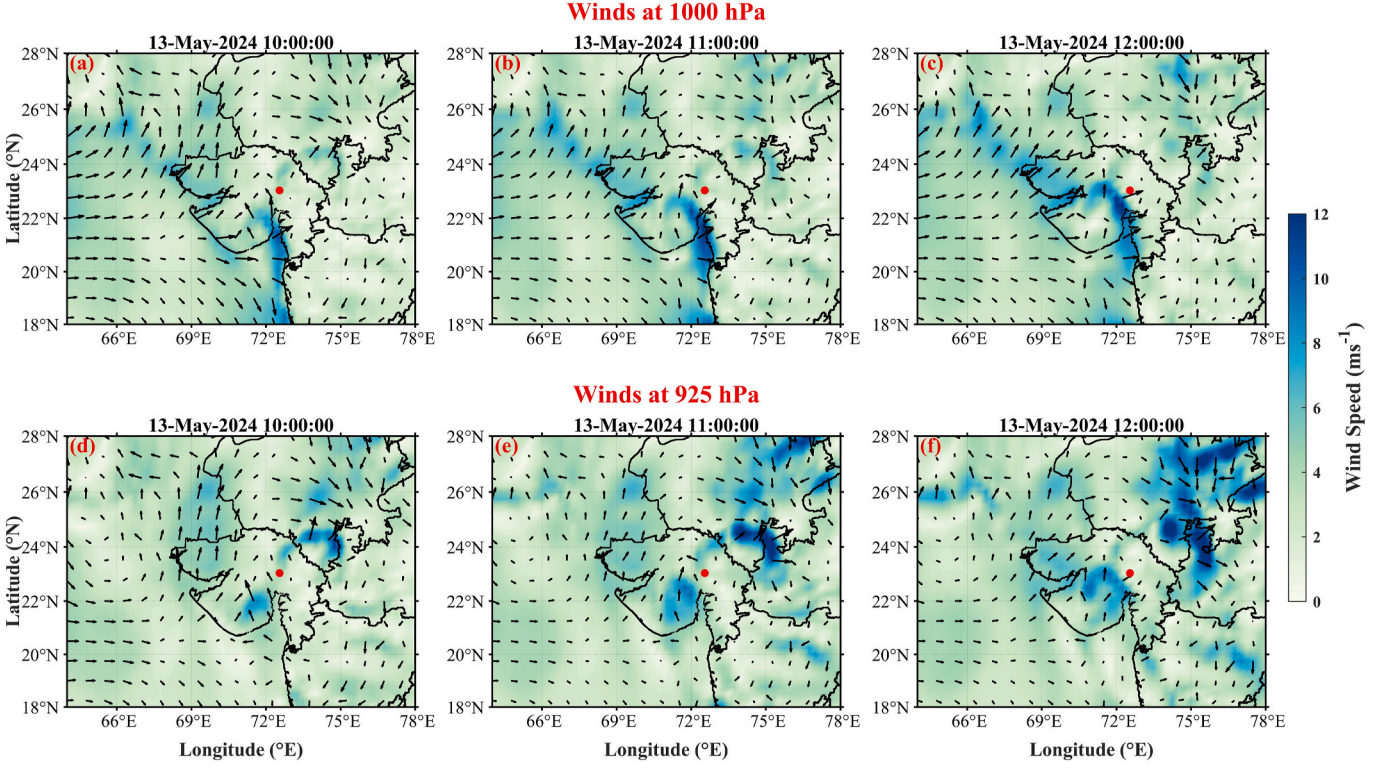

Fig. 7. ERA5 derived winds over the Western-Indian region on May 13, 2024 from 1000 UTC to 1200 UTC at 1000 hPa (top panel) and 925 hPa (bottom panel).

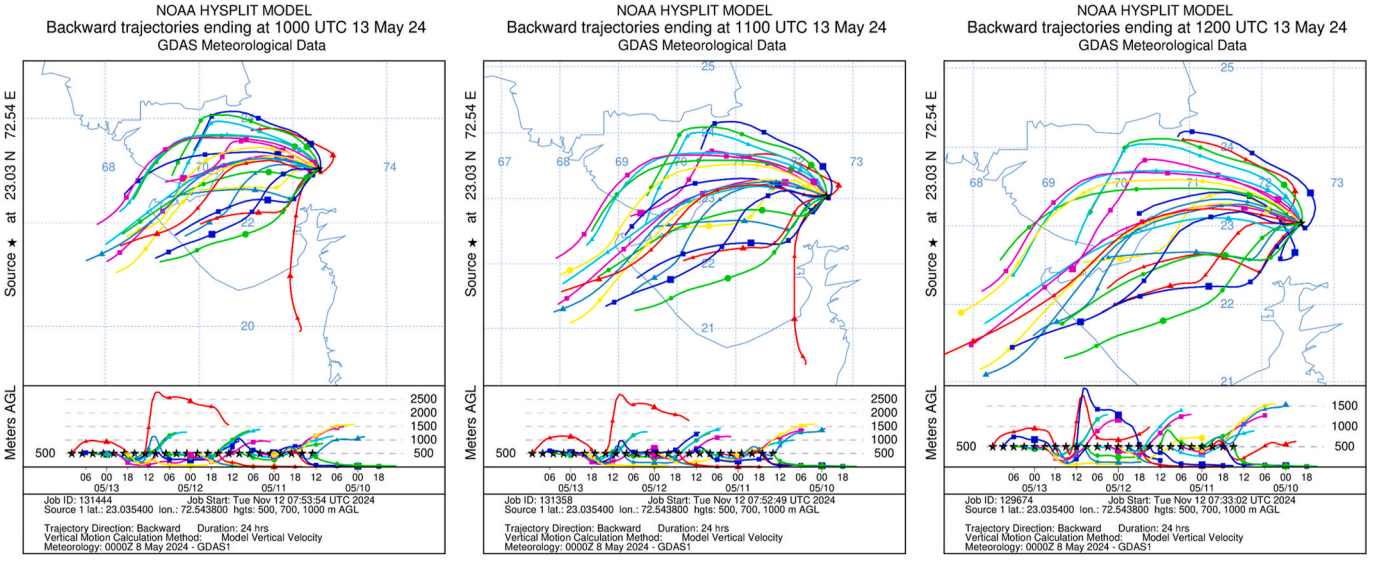

Fig. 8. One-day air mass back-trajectory ending at 500 m above ground level over Ahmedabad, from 1000 to 1200 UTC on May 13, 2024, generated using the HYSPLIT model.

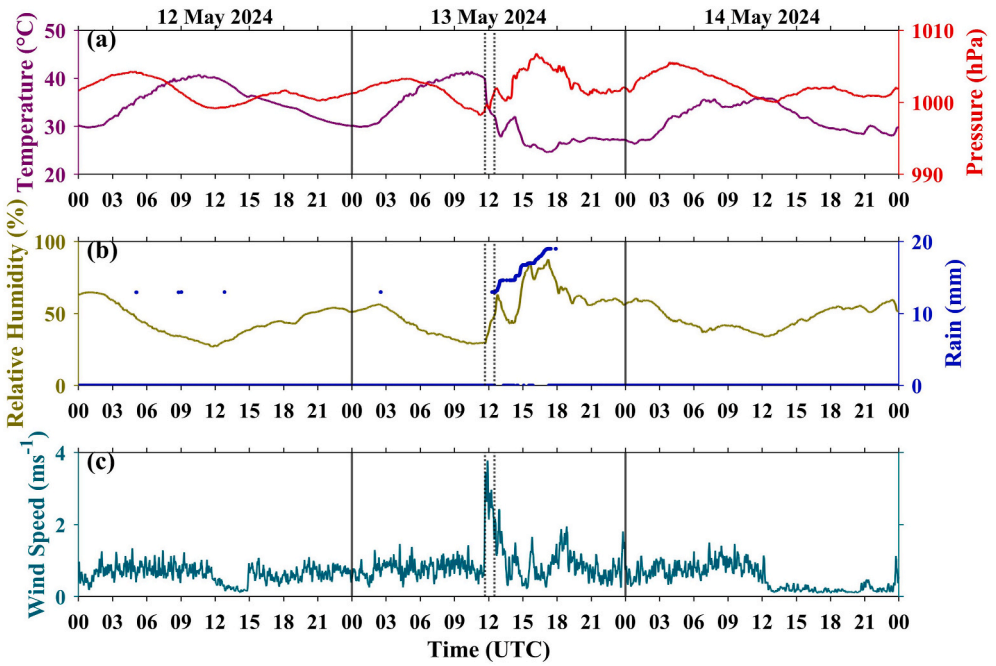

Fig. 9. Time series of meteorological parameters derived from the surface weather station setup at Physical Research Laboratory during 21–24 May 2024. The dust storm event is marked between the two black dotted lines on May 23, 2024.

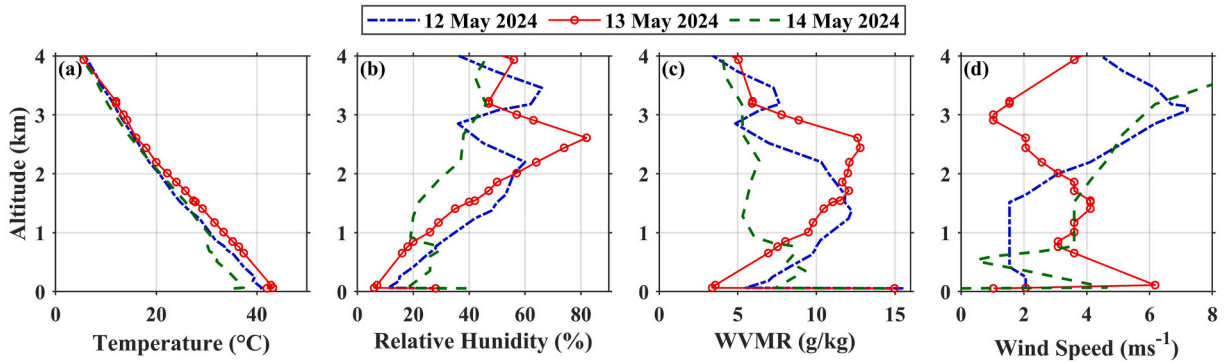

Fig. 10. Vertical profile of temperature, relative humidity, water vapor mixing ratio (WVMR), and wind speed over Ahmedabad on 12, 13, and May 14, 2024 at 1200 UTC derived from the radiosonde.

Table 1
Cloud properties derived from the MODIS, VIIRS/NOAA-20, and VIIRS/SNPP on May 13, 2024 over the Western-Indian region.

Time (Latitude, Longitude)	Instrument/ Satellite	Cloud Effective Radius (μm)	Cloud Optical Thickness	Cloud Water Path (gm^{-2})	Cloud Top Height (m)
2024-05-13 08:35 (22.00 °N,72.40 °E)	MODIS	17.92	137	1497	14337
2024-05-13 08:48 (22.00 °N, 72 °E)	VIIRS SNPP	13.12	150	1187	13161
2024-05-13 09:12 (22.00 °N, 72 °E)	VIIRS NOAA-20	16.82	150	1529	15972
2024-05-13 07:36 (24.61 °N,73.67 °E)	VIIRS NOAA-20	14.43	8	70	12904
2024-05-13 08:48 (24.61 °N,73.67 °E)	VIIRS SNPP	16.65	127	1284	13132
2024-05-13 09:30 (24.61 °N,73.67 °E)	MODIS	13.35	150	1209	13846

illustrates the vertical profile of various meteorological parameters from 12 May to 14 May 2024, at 1200 UTC. A dust storm impacted the study site on May 13, 2024, between 1140 and 1210 UTC, thus these vertical profiles represent conditions during the dust storm event. The temperature profile remained consistent across all three days, with the highest temperatures recorded on the day of the dust storm and the lowest on the day after the storm (Fig. 10a). During the dust storm, relative humidity increased gradually from 7% at the surface to 82% at approximately 2.6 km altitude (Fig. 10b). As discussed in Section 3.2, clouds were observed at ~2.7 km after the dust storm using the Ceilometer. This maximum relative humidity at that height suggests cloud formation. The water vapor mixing ratio (WVMR) also showed a similar trend, increasing from the surface to about 2.6 km and reaching 12.62 g/kg. The WVMR was higher on May 12, 2024, and lower on May 14, 2024, likely due to rainfall on May 13, 2024 (Fig. 10c). Near-surface wind speed was lowest on May 12, at approximately 2 m/s, and increased to around 6 m/s at 100 m height on the day of the storm (Fig. 10d).

3.4. Dust and cloud interaction

The dust storm originating from two moist convection systems in the Western-Indian region led to extensive cloud formation that spread across large parts of the Rajasthan and Gujarat, ultimately resulting in precipitation. Table 1 presents the properties of clouds formed during the event, as observed by the MODIS and VIIRS instruments. Deep convective clouds with top heights ranging from 13 to 16 km were observed moving towards the Ahmedabad region from the southwest. These clouds exhibited a cloud water path of approximately 1530 g/m^2 and an optical thickness of about 150. Similarly, strong convection in southeastern Rajasthan generated clouds with a significant vertical extent of around 11 km, an optical thickness of 150, and a cloud water path near 1209 g/m^2, as recorded by MODIS. These observations closely aligned with data from the VIIRS instrument onboard the Suomi National Polar-orbiting Partnership (SNPP) satellite. These deep convective clouds associated with the dust storm resulted in intense precipitation over the Ahmedabad region. Dust interacts with the clouds and can change its microphysical properties and subsequent precipitation (Yin et al., 2002; Bangert et al., 2012; Huang et al., 2018; Weger et al., 2018; Feng et al., 2023). Insoluble dust particles become more effective cloud condensation nuclei (CCN) after acquiring a sulphate layer in convective clouds, enhancing drop activation and precipitation formation in subsequent clouds (Yin et al., 2002). Dust particles can enhance extreme precipitation by promoting ice cloud formation and boosting convection. They act as ice nuclei in the upper troposphere, supporting ice cloud development and intensifying convection through latent heat release (Feng et al., 2023). These observations highlight the significant impact of the dust storm on cloud formation and properties in the region. The data from MODIS and VIIRS provide valuable insights into the microphysical properties of the clouds associated with such atmospheric events.

4. Summary and conclusions

The study investigated a sudden dust storm that occurred over Ahmedabad, a Western-India region, on the evening of May 13, 2024. This event was attributed to the outflow of two convective systems originating from the southwest part of Gujarat and the southeast part of Rajasthan. The movement of these convective systems, along with the dust storm, was effectively captured by the imager onboard geostationary satellite INSAT-3D and the MODIS instruments aboard NASA's Aqua and Terra satellites. The dynamics of the atmospheric boundary layer (ABL) during the dust storm were analyzed using ground-based Ceilometer Lidar. It was observed that the ABL underwent a significant transformation upon the arrival of the dust storm. The previously mixed layer, which extended to approximately 2.5 km during the daytime on 13 May, collapsed abruptly to about 250 m from the surface. The ABL continued to show altered characteristics on 14 May, with a shallower boundary layer and indications of high dust and aerosol concentration as inferred from strong backscatter signals. Vertical visibility during the dust storm drastically reduced to between 340 m and 660 m. Following the dust storm, clouds formed with a base height around 2.7 km, reaching updrafts of about 7.6 km and persisting throughout the night of 13 May. These clouds subsequently brought approximately 19 mm of rainfall, with nearly 15 mm falling within just 1 h over Ahmedabad. Analysis of cloud properties using MODIS and VIIRS instruments revealed these to be deep convective clouds with a vertical extent of approximately 11 km, characterized by a cloud optical thickness of 150 and a cloud water path of 1209 gm^{-2}. Surface meteorological conditions during 12–14 May 2024 were examined using a ground-based weather sensor collocated with the Ceilometer Lidar. Maximum surface temperatures peaked at 42 °C on the day of the dust storm, showing a slight increase of 1 °C compared to the previous day. However, temperatures decreased sharply by 5 °C on the subsequent day, suggesting a cooling effect attributed to dust particles interacting with incoming solar radiation. This cooling effect was also reflected in the shallowing of the boundary layer observed post-storm. The study highlighted the abrupt increase in relative humidity near the surface from 29% to 48% during the dust storm, attributed to moisture transport accompanying the dust. Radiosonde measurements indicated a vertical increase in relative humidity from 7% at the surface to 82% at approximately 2.6 km altitude leading to cloud formation. Strong winds with speeds around 6 m/s at 100 m altitude were recorded during the storm. Overall, this study underscores the role of moist convection in triggering sudden dust storms and influencing boundary layer dynamics. It emphasizes the critical importance of ground-based instruments, satellite observations, and reanalysis datasets in monitoring and studying the impact of dust storms on the atmosphere.

CRediT authorship contribution statement

Dharmendra Kumar Kamat: Writing – original draft, Validation, Methodology, Formal analysis, Conceptualization. **Som Kumar Sharma:** Writing – original draft, Supervision, Resources, Conceptualization. **Prashant Kumar:** Writing – original draft, Methodology. **Kondapalli Niranjan Kumar:** Writing – original draft, Formal analysis. **Aniket:** Methodology, Formal analysis, Data curation. **Sourita Saha:** Writing – original draft, Formal analysis. **Hassan Bencherif:** Writing – original draft, Supervision.

Data availability

The datasets used in this study are freely available and can be downloaded from the following: INSAT-3D brightness temperature product from MOSDAC: http://www.mosdac.gov.in/; Reflectance and cloud properties from MODIS and VIIRS: https://ladsweb.modaps.eosdis.nasa.gov/; Wind products from ERA5 Reanalysis: https://cds.climate.copernicus.eu/; Radiosonde data: https://weather.uwyo.edu/upperair/sounding.html. Ceilometer data will be made available on reasonable request.

Funding

The authors declare that no funds, grants, or other support were received during the preparation of this manuscript. The authors have no relevant financial or non-financial interests to disclose.

Declaration of competing interest

The authors declare that they have no known competing financial interests or personal relationships that could have appeared to influence the work reported in this paper.

Acknowledgement

The authors are thankful to the anonymous reviewers for their valuable comments and suggestions. We are grateful to Prof. Anil Bhardwaj, Director, Physical Research Laborator for helping in setting up the Lidar laboratory at Ahmedabad. Authors acknowledge MOSDAC for INSAT-3D data. We are also thankful to NASA and NOAA for MODIS and VIIRS cloud products freely available at https://ladsweb.modaps.eosdis.nasa.gov/. Authors are thankful to the ECMWF for providing ERA5 data, freely available at https://cds.climate.copernicus.eu/. This work is supported by the Physical Research Laboratory, Department of Space, Government of India.

References

Aghababaeian, H., Ostadtaghizadeh, A., Ardalan, A., Asgary, A., Akbary, M., Yekaninejad, M.S., Stephens, C., 2021. Global health impacts of dust storms: a systematic review. Environ. Health Insights 15, 11786302211018390.

Banerjee, P., Satheesh, S.K., Moorthy, K.K., 2021. The unusual severe dust storm of May 2018 over northern India: genesis, propagation, and associated conditions. J. Geophys. Res. Atmos. 126, e2020JD032369.

Bangert, M., Nenes, A., Vogel, B., Vogel, H., Barahona, D., Karydis, V.A., Kumar, P., Kottmeier, C., Blahak, U., 2012. Saharan dust event impacts on cloud formation and radiation over Western Europe. Atmos. Chem. Phys. 12, 4045–4063.

Bou, Karam D., Flamant, C., Knippertz, P., Reitebuch, O., Pelon, J., Chong, M., Dabas, A., 2008. Dust emissions over the Sahel associated with the West African monsoon intertropical discontinuity region: a representative case-study. Q. J. R. Meteorol. Soc. 134, 621–634.

Cao, C., Blonski, S., Wang, W., Uprety, S., Shao, X., Choi, J., Lynch, E., Kalluri, S., 2018. NOAA-20 VIIRS on-orbit performance, data quality, and operational Cal/Val support. In: Earth Observing Missions and Sensors: Development, Implementation, and Characterization V. SPIE, pp. 63–71.

Chakravarty, K., Vincent, V., Vellore, R., Srivastava, A.K., Rastogi, A., Soni, V.K., 2021. Revisiting Andhi in northern India: a case study of severe dust-storm over the urban megacity of New Delhi. Urban Clim. 37, 100825.

Chen, H., Sun, C., Xiong, X., Sarid, G., Sun, J., 2021. SNPP VIIRS day night band: ten years of on-orbit calibration and performance. Rem. Sens. 13, 4179.

Chhabra, A., Turakhia, T., Chauhan, P., 2021. Impacts of a mesoscale dust storm on aerosols characteristics, optical and radiative properties over a semiarid region, western India. J. Indian Soc. Rem. Sens. 49, 2133–2141.

Choi, H., Zhang, Y.H., Kim, K.H., 2008. Sudden high concentration of TSP affected by atmospheric boundary layer in Seoul metropolitan area during duststorm period. Environ. Int. 34, 635–647.

Choobari, O.A., Zawar-Reza, P., Sturman, A., 2014. The global distribution of mineral dust and its impacts on the climate system: a review. Atmos. Res. 138, 152–165.

Di, A., Xue, Y., Yang, X., Leys, J., Guang, J., Mei, L., Wang, J., She, L., Hu, Y., He, X., Che, Y., Fan, C., 2016. Dust aerosol optical depth retrieval and dust storm detection for Xinjiang Region using Indian national satellite observations. Rem. Sens. 8, 702.

Dumka, U.C., Kaskaoutis, D.G., Francis, D., Chaboureau, J.-P., Rashki, A., Tiwari, S., Singh, S., Liakakou, E., Mihalopoulos, N., 2019. The role of the intertropical discontinuity region and the heat low in dust emission and transport over the Thar Desert, India: a premonsoon case study. J. Geophys. Res. Atmos. 124, 13197–13219.

Evan, A.T., Heidinger, A.K., Pavolonis, M.J., 2006. Development of a new over-water advanced very high resolution radiometer dust detection algorithm. Int. J. Rem. Sens. 27, 3903–3924.

Feng, T., Yuan, T., Cao, J., Wang, Z., Zhi, R., Hu, Z., Huang, J., 2023. The influence of dust on extreme precipitation at a large city in North China. Sci. Total Environ. 901, 165890.

Fountoukis, C., Harshvardhan, H., Gladich, I., Ackermann, L., Ayoub, M.A., 2020. Anatomy of a severe dust storm in the Middle East: impacts on aerosol optical properties and radiation budget. Aerosol Air Qual. Res. 20, 155–165.

Frey, R.A., Ackerman, S.A., Liu, Y., Strabala, K.I., Zhang, H., Key, J.R., Wang, X., 2008. Cloud Detection with MODIS. Part I: Improvements in the MODIS Cloud Mask for Collection 5.

Garratt, J.R., 1994. The atmospheric boundary layer. Earth-Science Reviews 37 (1–2), 89–134.

Goudie, A.S., 2009. Dust storms: recent developments. J. Environ. Manag. 90, 89–94.

Goudie, A.S., 2020. Dust storms and human health. In: Akhtar, R. (Ed.), Extreme Weather Events and Human Health: International Case Studies. Springer International Publishing, Cham, pp. 13–24.

Hersbach, H., Bell, B., Berrisford, P., Hirahara, S., Horányi, A., Muñoz-Sabater, J., Nicolas, J., Peubey, C., Radu, R., Schepers, D., Simmons, A., Soci, C., Abdalla, S., Abellan, X., Balsamo, G., Bechtold, P., Biavati, G., Bidlot, J., Bonavita, M., De, Chiara G., Dahlgren, P., Dee, D., Diamantakis, M., Dragani, R., Flemming, J., Forbes, R., Fuentes, M., Geer, A., Haimberger, L., Healy, S., Hogan, R.J., Hólm, E., Janisková, M., Keeley, S., Laloyaux, P., Lopez, P., Lupu, C., Radnoti, G., de Rosnay, P., Rozum, I., Vamborg, F., Villaume, S., Thépaut, J.-N., 2020. The ERA5 global reanalysis. Q. J. R. Meteorol. Soc. 146, 1999–2049.

Huang, Z., Nee, J.-B., Chiang, C.-W., Zhang, S., Jin, H., Wang, W., Zhou, T., 2018. Real-time observations of dust–cloud interactions based on polarization and Raman Lidar measurements. Rem. Sens. 10, 1017.

Huang, J., Wang, T., Wang, W., Li, Z., Yan, H., 2014. Climate effects of dust aerosols over East Asian arid and semiarid regions. J. Geophys. Res. Atmos. 119 (11), 398-11,416.

Jasim, S.A., Mohammadi, M.J., Patra, I., Jalil, A.T., Taherian, M., Abdullaeva, U.Y., Sharma, S., Ekrami, H.A., Mousavion, K., Alborzi, M., 2022. The effect of microorganisms (bacteria and fungi) in dust storm on human health. Rev. Environ. Health 39, 65–75.
Karydis, V.A., Kumar, P., Barahona, D., Sokolik, I.N., Nenes, A., 2011. On the effect of dust particles on global cloud condensation nuclei and cloud droplet number. J. Geophys. Res. Atmos. 116.
Kedia, S., Kumar, R., Islam, S., Sathe, Y., Kaginalkar, A., 2018. Radiative impact of a heavy dust storm over India and surrounding oceanic regions. Atmos. Environ. 185, 109–120.
Khaniabadi, Y.O., Daryanoosh, S.M., Amrane, A., Polosa, R., Hopke, P.K., Goudarzi, G., Mohammadi, M.J., Sicard, P., Armin, H., 2017. Impact of middle eastern dust storms on human health. Atmos. Pollut. Res. 8, 606–613.
Knippertz, P., 2014. Meteorological aspects of dust storms. In: Knippertz, P., Stuut, J.-B.W. (Eds.), Mineral Dust: A Key Player in the Earth System. Springer, Dordrecht, pp. 121–147. Netherlands.
Kumar, R., Barth, M.C., Pfister, G.G., Naja, M., Brasseur, G.P., 2014. WRF-Chem simulations of a typical pre-monsoon dust storm in northern India: influences on aerosol optical properties and radiation budget. Atmos. Chem. Phys. 14, 2431–2446.
Kumar, S., Kumar, S., Kaskaoutis, D.G., Singh, R.P., Singh, R.K., Mishra, A.K., Srivastava, M.K., Singh, A.K., 2015. Meteorological, atmospheric and climatic perturbations during major dust storms over Indo-Gangetic Basin. Aeolian Res. 17, 15–31.
Kumar, P., Nenes, A., Sokolik, I.N., 2009. Importance of adsorption for CCN activity and hygroscopic properties of mineral dust aerosol. Geophys. Res. Lett. 36.
Kumar, P., Shukla, M.V., 2019. Assimilating INSAT-3D thermal infrared window imager observation with the particle filter: a case study for Vardah Cyclone. J. Geophys. Res. Atmos. 124, 1897–1911.
Liang, S., Fang, H., Chen, M., Shuey, C.J., Walthall, C., Daughtry, C., Morisette, J., Schaaf, C., Strahler, A., 2002. Validating MODIS land surface reflectance and albedo products: methods and preliminary results. Rem. Sens. Environ. 83, 149–162.
Lo, Feudo T., Calidonna, C.R., Avolio, E., Sempreviva, A.M., 2020. Study of the vertical structure of the coastal boundary layer integrating surface measurements and ground-based remote sensing. Sensors 20, 6516.
Möhler, O., Field, P.R., Connolly, P., Benz, S., Saathoff, H., Schnaiter, M., Wagner, R., Cotton, R., Krämer, M., Mangold, A., Heymsfield, A.J., 2006. Efficiency of the deposition mode ice nucleation on mineral dust particles. Atmos. Chem. Phys. 6, 3007–3021.
Münkel, C., Eresmaa, N., Räsänen, J., Karppinen, A., 2007. Retrieval of mixing height and dust concentration with lidar ceilometer. Boundary-Layer Meteorol. 124, 117–128.
Parambil, L.P., Kumar, V.A., Vijayakumar, K., Basheer, A.I., Sravanthi, N., Patil, R.D., Pandithurai, G., 2023. Aerosol-CCN characteristics and dynamics associated with a pre-monsoon dust storm over a high-altitude site in Western Ghats, India. Environ. Sci. Pollut. Res. 30, 109372–109388.
Platnick, S., King, M.D., Ackerman, S.A., Menzel, W.P., Baum, B.A., Riedi, J.C., Frey, R.A., 2003. The MODIS cloud products: algorithms and examples from Terra. IEEE Trans. Geosci. Rem. Sens. 41, 459–473.
Prakash, D., Payra, S., Verma, S., Soni, M., 2013. Aerosol particle behavior during Dust Storm and Diwali over an urban location in north western India. Nat. Hazards 69, 1767–1779.
Qu, J.J., Hao, X., Kafatos, M., Wang, L., 2006. Asian dust storm monitoring combining Terra and Aqua MODIS SRB measurements. Geosci. Rem. Sens. Lett. IEEE 3, 484–486.
Saha, S., Sharma, S., Chhabra, A., Kumar, K.N., Kumar, P., Kamat, D., Lal, S., 2022. Impact of dust storm on the atmospheric boundary layer: a case study from western India. Nat. Hazards 113, 143–155.
Santra, P., Kumar, S., Roy, M.M., 2018. Thar Desert: source for dust storm. In: Natural Hazards. CRC Press.
Shao, Y., Dong, C.H., 2006. A review on East Asian dust storm climate, modelling and monitoring. Global Planet. Change 52, 1–22.
Sharma, D., Singh, D., Kaskaoutis, D.G., 2012. Impact of two intense dust storms on aerosol characteristics and radiative forcing over Patiala, Northwestern India. Adv. Meteorol. 2012, 956814.
Shukla, K.K., Attada, R., Khan, A.W., Kumar, P., 2022. Evaluation of extreme dust storm over the northwest Indo-Gangetic plain using WRF-Chem model. Nat. Hazards 110, 1887–1910.
Shukla, K.K., Sharma, S.K., Kumar, K.N., Kumar, P., Kamat, D.K., Attada, R., Saha, S., 2023. Characterization of a regional dust storm using Raman Lidar over the western Indian region. J. Indian Soc. Rem. Sens. 51, 2549–2559.
Singh, J., Singh, N., Ojha, N., Srivastava, A.K., Bisht, D.S., Rajeev, K., Kumar, K.N.V.P., Singh, R.S., Panwar, V., Dhaka, S.K., Kumar, V., Nakayama, T., Matsumi, Y., Hayashida, S., Dimri, A.P., 2022. Genesis of a severe dust storm over the Indian subcontinent: dynamics and impacts. Earth Space Sci. 9, e2021EA001702.
Slingo, A., Ackerman, T.P., Allan, R.P., Kassianov, E.I., McFarlane, S.A., Robinson, G.J., Barnard, J.C., Miller, M.A., Harries, J.E., Russell, J.E., Dewitte, S., 2006. Observations of the impact of a major Saharan dust storm on the atmospheric radiation balance. Geophys. Res. Lett. 33.
Stein, A.F., Draxler, R.R., Rolph, G.D., Stunder, B.J.B., Cohen, M.D., Ngan, F., 2015. NOAA's HYSPLIT Atmospheric Transport and Dispersion Modeling System.
Sun, K., Su, Q., Ming, Y., 2019. Dust storm remote sensing monitoring supported by MODIS land surface reflectance database. Rem. Sens. 11, 1772.
Wang, T., Tang, J., Sun, M., Liu, X., Huang, Y., Huang, J., Han, Y., Cheng, Y., Huang, Z., Li, J., 2021. Identifying a transport mechanism of dust aerosols over South Asia to the Tibetan Plateau: a case study. Sci. Total Environ. 758, 143714.
Weger, M., Heinold, B., Engler, C., Schumann, U., Seifert, A., Fößig, R., Voigt, C., Baars, H., Blahak, U., Borrmann, S., Hoose, C., Kaufmann, S., Krämer, M., Seifert, P., Senf, F., Schneider, J., Tegen, I., 2018. The impact of mineral dust on cloud formation during the Saharan dust event in April 2014 over Europe. Atmos. Chem. Phys. 18, 17545–17572.
Yin, Y., Wurzler, S., Levin, Z., Reisin, T.G., 2002. Interactions of mineral dust particles and clouds: effects on precipitation and cloud optical properties. J. Geophys. Res. Atmos. 107 (AAC 19-1-AAC 19-14).
Zhang, X., Zhao, L., Tong, D.Q., Wu, G., Dan, M., Teng, B., 2016. A systematic review of global desert dust and associated human health effects. Atmosphere 7, 158.